Journal of Power Sources 273 (2015) 511–516

Contents lists available at ScienceDirect

Journal of Power Sources

journal homepage: www.elsevier.com/locate/jpowsour

Enhanced performance of lithium sulfur battery with self-assembly polypyrrole nanotube film as the functional interlayer

Guoqiang Ma, Zhaoyin Wen*, Qingsong Wang, Chen Shen, Peng Peng, Jun Jin, Xiangwei Wu

CAS Key Laboratory of Materials for Energy Conversion, Shanghai Institute of Ceramics, Chinese Academy of Sciences, Shanghai 200050, PR China

HIGHLIGHTS

- Polypyrrole nanotube film (PNTF) is self-assembled with a simple method from PPy nano-tubes with high aspect ratio.
- PNTF is used as the functional interlayer for Li–S battery.
- Li–S battery with PNTF displays an enhanced cycling performance, even with high sulfur loading.

GRAPHICAL ABSTRACT

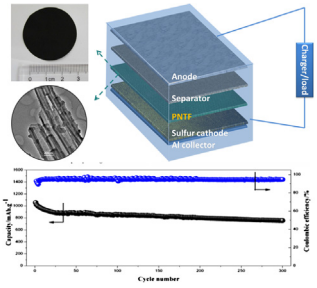

ARTICLE INFO

Article history:
Received 19 August 2014
Received in revised form
20 September 2014
Accepted 22 September 2014
Available online 30 September 2014

Keywords:
Lithium sulfur
Polypyrrole nanotube
Functional interlayer
Cycle performance

ABSTRACT

Polypyrrole nanotube film (PNTF) is self-assembled with a simple method from PPy nano-tubes. Consequently, PNTF is sandwiched between sulfur cathode and separator to act as the functional interlayer for Li–S battery. Because of the adsorption effect between PPy and lithium polysulfides and the conductivity of PPy films, the polymer interlayer can not only decrease the polarization of sulfur cathode significantly, but also suppress shuttle effect and the redistribution of active material during charge/discharge process effectively. Li–S battery with the functional interlayer shows an encouraging electrochemical performance. With approximately 2.5–3 mg cm^{-2} sulfur loading on the electrode, the initial discharge capacity is 1102 mAh g^{-1}, and the capacity retains at 712 mAh g^{-1} after 300 cycles at 0.5C, and the coulombic efficiency increases to around 92% in the electrolyte without $LiNO_3$.

1. Introduction

Currently, with rapid development in advanced portable devices, zero-emission electric vehicles (EV) and smart grids, rechargeable batteries with high energy density and long cycle life are in great demand [1,2]. Among various battery systems, sulfur cathode has a high theoretical capacity (1675 mAh g^{-1}) and a high theoretical specific energy (2600 Wh Kg^{-1}). In combination with the natural abundance, low cost and environmental friendliness of sulfur, the Lithium sulfur (Li–S) battery becomes a promising candidate for the next generation [3–5].

However, the insulating nature of sulfur, the volume expansion, and the high solubility of lithium polysulfides (PS) in the ether-based electrolyte lead to a high polarization, serious capacity fading, poor rate stability and low coulombic efficiency of Li–S battery, inhibiting its commercialization [6,7]. Many approaches have been made to address these obstacles and improve the eletrochemical performance of Li–S battery [3,6]. Most studies are focusing on the modification of cathode with various kinds of

* Corresponding author. Shanghai Institute of Ceramics, Chinese Academy of Sciences, 1295 DingXi Road, Shanghai 200050, PR China. Tel.: +86 21 52411704; fax: +86 21 52413903.
E-mail addresses: zywen@mail.sic.ac.cn, gxzhang@student.sic (Z. Wen).

http://dx.doi.org/10.1016/j.jpowsour.2014.09.141
0378-7753/

carbon materials and conductive polymers [8–10]. All the approaches can enhance the electrical conductivity of the cathode and suppress the loss of soluble polysulfides intermediates, and thereby improving the active material utilization and cycle stability. In addition, the issue of low coulombic efficiency is resolved by the modification of the electrolyte [11–14]. Although studies on the sulfur cathode show promising improvements, but the material processing steps are often complex and costly, limiting the feasibility of manufacturing a viable Li–S battery. Therefore, more effective approaches need to be set up for the commercialization of Li–S battery [2].

Recently, interlayers of micro-porous carbon paper [15], free standing MWCNT paper [16], reduced grapheme oxide based film [17], and treated carbon paper [18] have been incorporated between sulfur cathode and separator as the carbon interlayer. The carbon interlayer facilitates the adsorption of soluble lithium polysulfides and makes them available for reutilization during the following cycles. Moreover, the carbon interlayer can reduce the polarization of the cell significantly. The cycle performance is enhanced self-evidently with this simple strategy. However, the long-term cycle performance still needs to be improved owing to the weak adsorbing ability of carbon to lithium polysulfides.

It is reported that conductive polymers such as poly(3,4-ethylenedioxythiophene) (PEDOT) [19], polyaniline (PAN) [10,20,21], polypyrrole (PPy) [22,23], and polythiophene (PTh) [24] are usually proton-doped so that the protons can act as bridges to link the polymers to PS anions via H-bonds [5,25]. The H-bonds between the proton-doped polymers and lithium polysulfides make them adsorb PS more effectively during charge/discharge process. Meanwhile, the conductive polymers are both electronically and ionically conductive, which is beneficial to reduce the resistance and enhance the rate capability of the cell. Furthermore, the conductive polymers themselves are electrochemically active, which can provide some capacity for the cell. Thus conductive polymers are more suitable to be used as the functional interlayer for Li–S battery. Polypyrrole functional interlayer (PFIL) has been in-situ fabricated uniformly onto the surface of sulfur cathode to inhibit the dissolution of lithium polysulfides and protect sulfur cathode in our previous reports [26]. Li–S battery with PFIL showed enhanced cycle performance, however, the initial discharge capacity was decreased because of the dense interlayer, and it showed limited advantages in Li–S battery with high sulfur loading.

Herein, as seen in Fig. 1, PPy nanotubes film (PNTF) is self-assembled from PPy nano-tubes, which is sandwiched between the sulfur cathode and separator as the functional interlayer. Because of the H-bond and large specific area PPy nanotube, PNTF can inhibit the dissolution and migration of PS in the electrolyte effectively. PNTF can also protect the structure of sulfur cathode from being damaged during charge/discharge process. So the novel configuration presented here is more suitable to be applied to overcome the problems of Li–S battery.

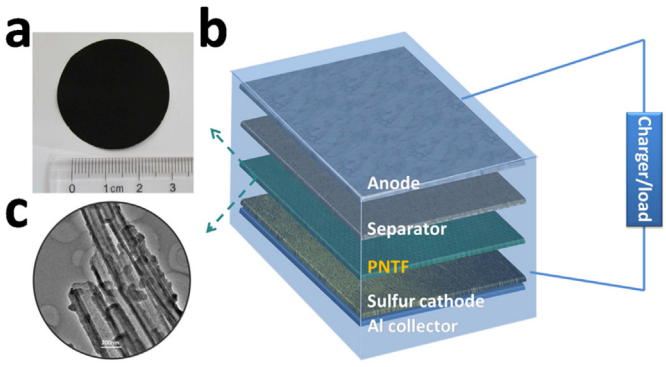

Fig. 1. (a) Images of the PPy nanotube film, (b) TEM images of and PPy nano-tubes, (c) a schematic cell configuration of rechargeable Li–S batteries.

2. Experimental

2.1. Preparation of the PPy nanotube film

The tubular polypyrrole (T-PPy) was synthesized by an improved self-degraded template method [27]. 200 ml aqueous solution of $Fe(NO_3)_3$ (50 mmol) and methyl orange (1 mmol) was prepared as the template. 10 mmol pyrrole was added into the template and stirred for 24 h. The BET surface area of PPy nanotube was as high as 289 $m^2\ g^{-1}$. The PPy nanotube film was obtained after vacuum filtration and drying. The product was washed by water and ethanol alternatively until the filtrate was colorless. The thickness of PNTF is around 35 μm, and the areal density is around 1 mg cm^{-2}.

2.2. Preparation of the sulfur cathode

The S/C composite was prepared by a melting diffusion strategy with a mixture of sulfur and Ketjen black (KB) (Akzo Nobel Corp.) in the weight ratio of 2:1. Then the composite was sealed in a glass tube under vacuum followed by co-heating at 155 °C for 12 h. Consequently, the slurry was prepared by ball milling 80% S/C composite, 10 wt% acetylene black (AB) as conductive agent, 5 wt% carboxy methyl cellulose (CMC), 5 wt% (styrene-butadiene rubber) SBR as binders and deionized water as the solvent. The slurries were casted onto aluminum foil substrates. After the solvent was evaporated, the electrode was cut into discs with 14 mm in diameter and then dried at 60 °C under vacuum for 12 h. To exclude the mass factor of the PFIL, the sulfur cathode with the same content of PPy nanotube was also prepared, (S:KB:PPy = 2.5:1.25:1.5). Accordingly, the sulfur loading in the cathode was around 2.5–3 mg cm^{-2}. CR2025 type coin cells were assembled in a glove box with oxygen and water contents less than 1 ppm. PPy nanotube films are sandwiched between sulfur cathode and separator to act as the functional interlayer. The electrolyte consisted of 1 M $LiN(CF_3SO_2)_2$ (LiTFSI) in a mixed solvent of 1,3-dioxolane (DOL) and dimethyl ether(DME). The cells contained Celgard 2400 as the separator and lithium foils as both the counter and reference electrodes.

2.3. Characterization

SEM images were measured by field emission scanning electron microscope (FESEM JSM-6700) and scanning electron microscope (Hitachi S-3400 N). AC impedance measurement was carried out by a Frequency Response Analyzer (FRA) technique on an Autolab Electrochemical Workstation over the frequency range from 0.1 Hz to 10 MHz with the amplitude of 10 mV. The galvanostatic charge and discharge tests were conducted on a LAND CT2001A battery test system in a voltage range of 1.8–2.8 V (vs. Li/Li^+).

3. Results and discussions

SEM images of PPy nanotubes fabricated though the modified soft template are shown in Fig. 2. As seen, uniform PPy nanotubes are obtained, the diameters and lengths of the PPy nanotubes are around 120 nm and 20 μm, respectively. The higher proportion of Fe^{3+} compared to MO during the fabrication process aims to obtain a higher aspect ratio of PPy nanotubes, which can improve the mechanical strength of the PNTF [28].

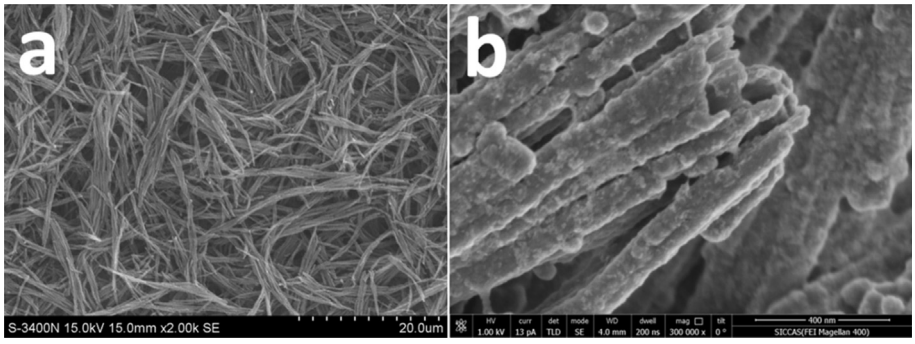

Fig. 2. The SEM images of PPy nanotube at different magnifications.

As seen in Fig. 3a, The cells displays close initial discharge capacities, because PNTF is porous, which can't hinder the perfect contact between the sulfur cathode and the electrolyte. The charge/discharge profiles of Li–S battery with and without PNTF show that there are two discharge plateaus at around 2.3 V and 2.1 V corresponding to the generating of Li_2S_x ($x > 2$) and Li_2S_y ($y \leq 2$), respectively [29]. However, Li–S battery with PNTF shows higher discharge plateaus and lower charge plateaus relatively, indicating a decreased polarization. It is worth noting that there is a valley at the end of the first discharge plateau and a peak at the beginning of the charge profile for the cell without interlayer, while they both disappear for the cell with PNTF. The viscosity of the electrolyte reaches the maximum value because of the dissolution of lithium polysulfides at the end of the first plateau in the electrolyte, which increases the polarization of the battery. The dissolved lithium polysulfides are reduced to the insoluble Li_2S_2/Li_2S, then the viscosity of the electrolyte decreases at the beginning of the second discharge plateau, which weakens the polarization of the battery, so there is a valley at the end of the first discharge plateau. The peak at the beginning of the charge profiles is also attributed to the changes of the polarization. The redistribution of insulating sulfur can't be avoided because of the dissolution of lithium polysulfides during the charge/discharge process. It increases the polarization of Li–S battery when the Li_2S/Li_2S_2 insulating layer is formed on the

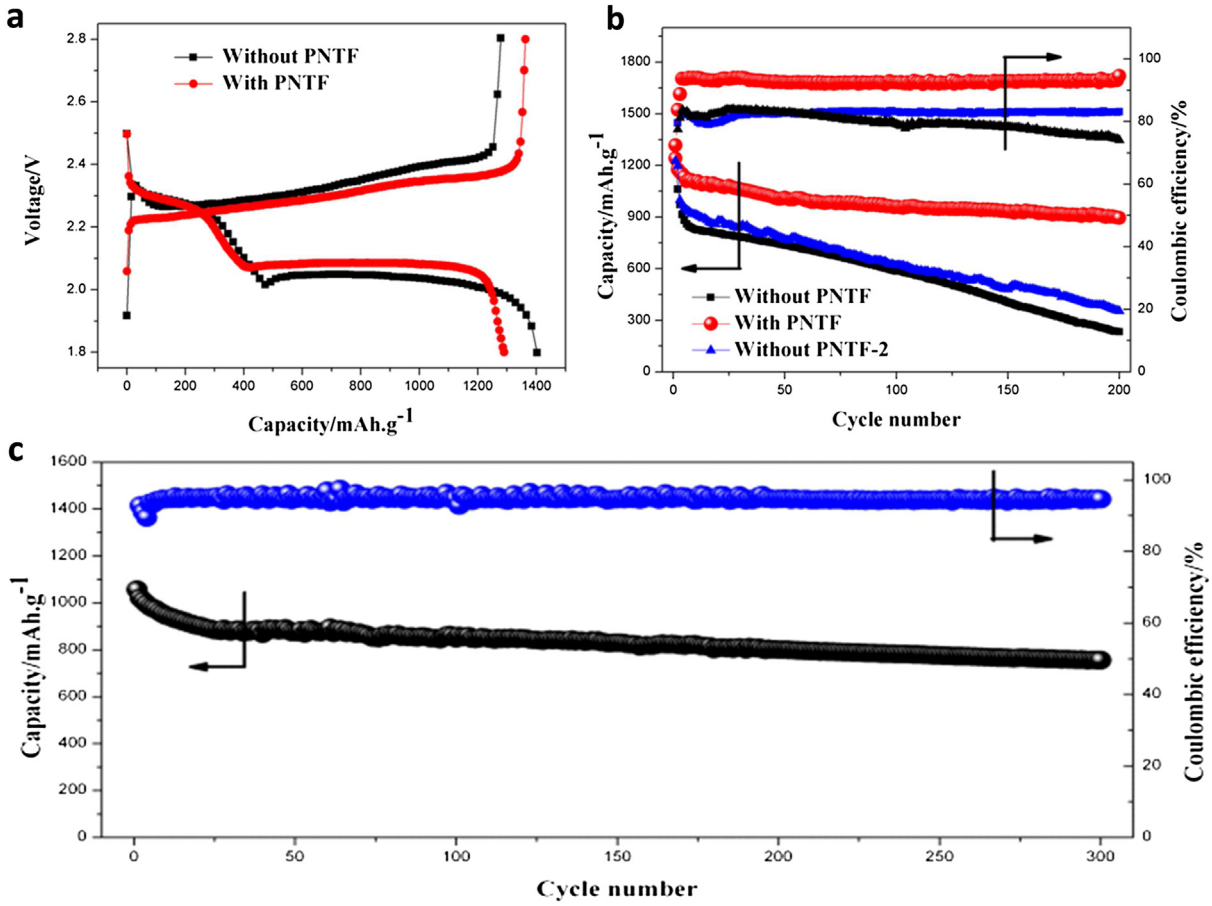

Fig. 3. (a) Initial charge/discharge profiles, (b) cycle performance and coulombic efficiency of Li–S batteries with PNTF and without PNTF at 0.2C, (c) the prolonged cycle performance of Li–S battery with PNTF at 0.5C.

Table 1
Fitted values of the impedance spectra in Fig. 4, R_e, R_{ct} and R_{int} correspond to Fig. 4a, R'_e, R'_{ct} and R'_{int} correspond to Fig. 4b.

	$R_e(\Omega)$	$R_{ct}(\Omega)$	$R_{int}(\Omega)$	$R'_e(\Omega)$	$R'_{ct}(\Omega)$	$R'_{int}(\Omega)$
0 cycle	3.74	69.3	15	3.68	29.5	12
5 cycle	4.34	2.5	6.2	4.02	2.5	8.5
15cycle	5.39	2.7	8.4	4.52	2.7	8.2
30 cycle	6.43	3.1	11.1	5.12	3	8.3
60 cycle	7.63	6.2	13.1	6.50	3.2	9.5
100 cycle	8.85	11.4	14.6	7.35	3.3	10.2

surface of cathode, anode and separator at the end of the discharge process. Then the insulating layer is transformed to the soluble lithium polysulfides at the beginning of the charge process, resulting in the peak at the beginning of the charge process [30]. Both the two phenomenon disappear because of the addition of PNTF, indicating that PNTF can effectively suppress dissolution of lithium polysulfides and the redistribution of insulating active material, then the polarization changing during the charge/discharge process is suppressed.

Fig. 3b shows the cycle performance and coulombic efficiency of the cells with and without PNTF. There is strong adsorption effect between PPy and lithium polysulfides, in addition to the large specific areas of PPy nano-tube. Therefore, as the functional interlayer, PNTF can inhibit the dissolution and migration of lithium polysulfides more effectively than carbon materials based interlayer, then shuttle effect is suppressed effectively. So the low coulombic efficiency and attenuated capacity fading owing to shuttle effect are inhibited. The discharge capacity of Li–S batteries with PNTF retains at 890 mAh g^{-1} at 0.2C after 200 cycles, which is much higher than the cell without interlayer (287 mAh g^{-1} after 200 cycles). Simultaneously, the average coulombic efficiencies of Li–S batteries with PNTF are as high as 90.89%, which is higher than that of the cell without PNTF. To exclude the mass factor of the PNTF, the cycle performance of sulfur cathode with the same sulfur content compared to the sulfur cathode with PNTF is shown in Fig. 3b (without PNTF-2), too. As seen, the cycle performance is enhanced to some extent with the addition of PPy nanotubes in the cathode directly, because the sulfur content decreases. While it is far worse than the cell with PNTF, so the enhanced electrochemical performance can be attributed to the addition of PNTF. Moreover, PNTF shows enhanced improvement performance compared to that of PFIL [26], because of the higher specific area and the pores of PNTF, which has stronger adsorption effect, and it wouldn't hinder the contact between the sulfur cathode and electrolyte.

As seen in Fig. 3c, the initial discharge capacity is 1102 mAh g^{-1}, and it retains at 712 mAh g^{-1} after 300 cycles at 0.5C, and the coulombic efficiency increase to around 92% in the electrolyte without $LiNO_3$. Although the addition of $LiNO_3$ in the electrolyte can increases the coulombic efficiency of Li–S battery, it has been reported that the electrolyte with $LiNO_3$ added can oxidize sulfur compounds to higher and irreversible oxidation states, such as Li_xSO_y species [31]. Moreover, the decomposition of $LiNO_3$ will generate gas during charge/discharge. The Li–S battery with PNTF shows excellent cycle stability and improved coulombic efficiency in the electrolyte without $LiNO_3$. which can avoid the disadvantages of $LiNO_3$ additives. Table 1.

To investigate the electrochemical process of Li–S battery with and without PNTF, the Nyquist plots of the cells at fully charged state after different cycles are carried out on an Autolab. As shown in Fig. 4, the Nyquist plots of Li–S battery is composed of a depressed semicircle in the high frequency region (corresponding to the interfacial resistance R_{int}), a depressed semicircle in middle frequency region (corresponding to the charge transfer resistance R_{ct}) and a straight slopping line in the low frequency region (corresponding to the Warburg resistance) [32,33]. The fitted values of the impedance spectra in Fig. 4 are shown in Table. For the Li–S battery with and without PNTF, the resistance decreases largely after 5 cycles, indicating the electrochemical activity. Hereafter, the R_{ct} and R_{int} increase evidently because of the redistribution of insulating active material on the surface of cathode, anode or separator during charge/discharge process, The increased R_e can be attributed to the dissolved lithium polysulfides in the electrolyte, which increases the viscosity of the electrolyte. For Li–S battery with PNTF, PPy interlayer act as a pseudo-upper current collector, reducing the effective resistance of the highly insulating sulfur cathodes [16]. And the increase of R'_e is inhibited, showing the suppressing of the dissolution of lithium polysulfides. R'_{ct} and R'_{int} retain at around 3 Ω and 10 Ω, respectively, showing the inhabitation of the redistribution of insulating sulfur with the addition of PNTF during charge/discharge process.

To further determine the adsorption effect of PPy to PS and S, the surface morphology of the PNTF after 100 cycles is observed in Fig. 5. There are some deposition on the surface of PNTF, and the diameter of cycled PPy nanotubes is around 180 nm, which is larger than that of PPy nano-particles fabricated before with the same

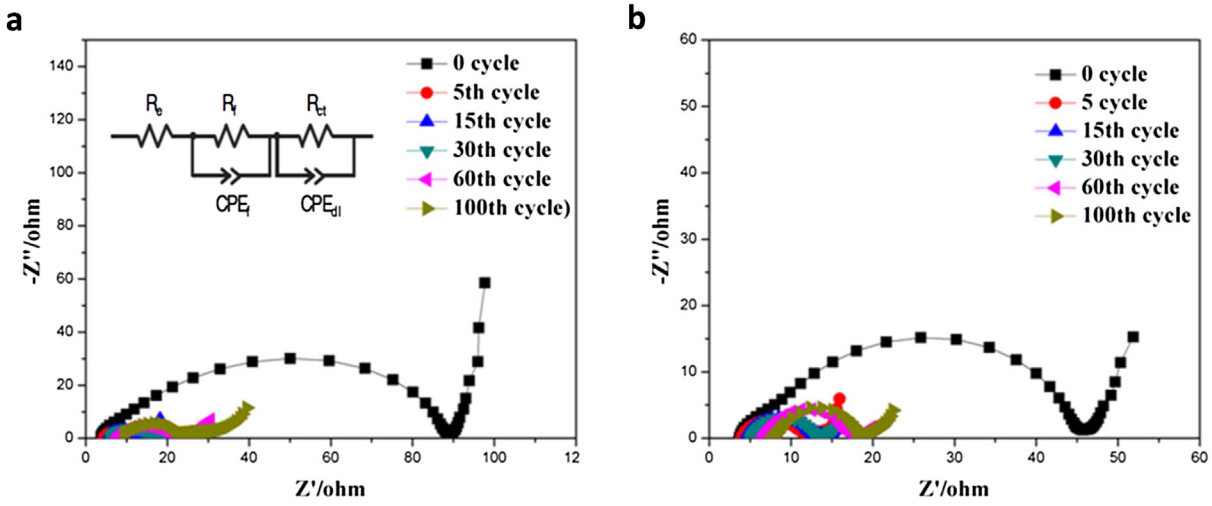

Fig. 4. Nyquist plots measured at different cycles of Li–S battery with PNTF(a) and without PNTF(b).

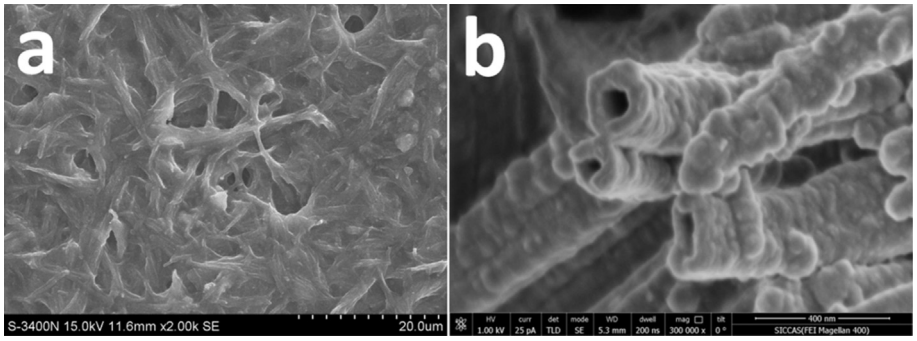

Fig. 5. The SEM images of PNTF after 100cycles at 0.2C.

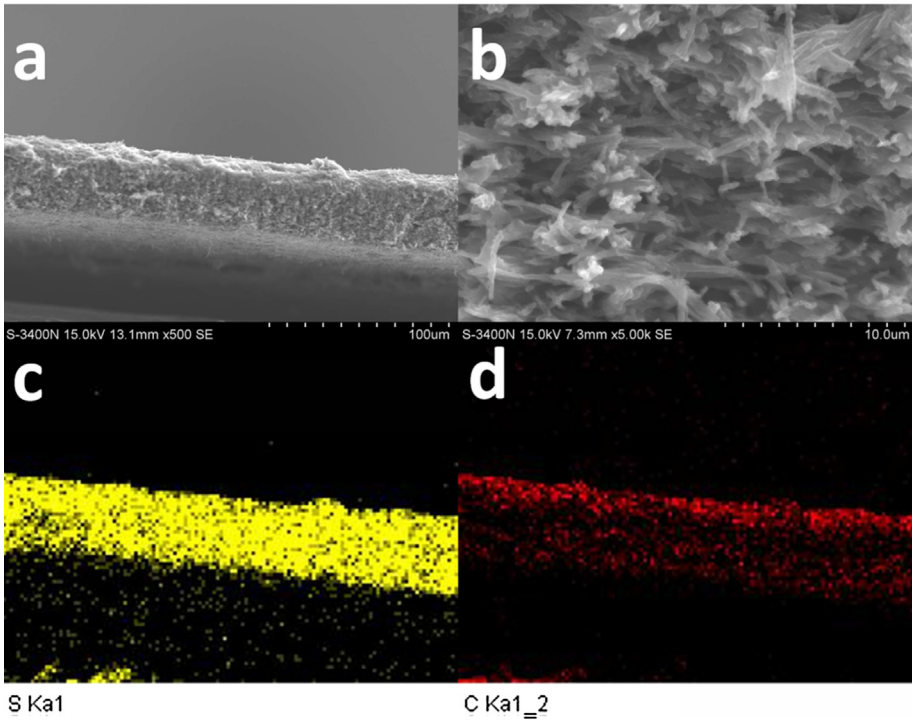

Fig. 6. The cross-sectional morphology of PNTF after 100cycles at 0.2C (a), (b), the elemental mapping of S (c) and C (d) in (a).

method (as shown in Fig. 2), showing the deposition of active material. The cross-section morphology and elemental mapping of PNTF are shown Fig. 6, as shown, the thickness of PNTF is around 35 μm, and the C and S elements have the same distribution as the section of PNTF, suggesting that there is elemental sulfur coating onto the surface of PPy nano-particles. It was reported that not all the Li_2S can be oxidized to sulfur during charge process, so the material coated on the surface of PNTF consist of sulfur and lithium polysulfides [5].

Because of the addition of PNTF, the corrosion reaction on the surface of anode is suppressed evidently. As shown in Fig. 7a, the surface of the pristine lithium sheet is smooth, while it becomes uneven and loosely packed after 100 cycles, suggesting serious corrosion of lithium anode during charge/discharge process [13,34].

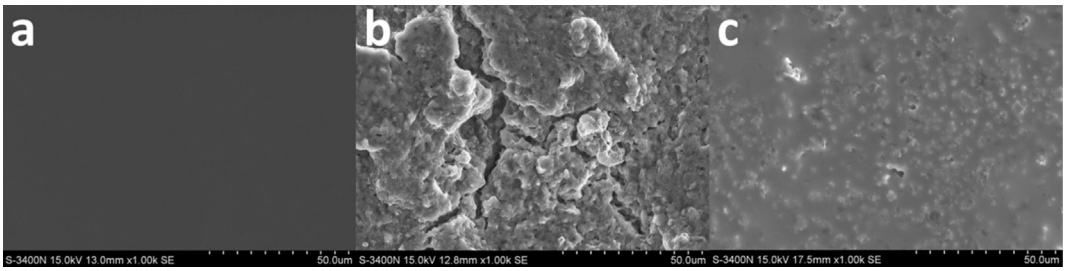

Fig. 7. The SEM image of the pristine Li anode (a), the Li anode after 100cycles without PNTF (b), and the Li anode after 100cycles with PNTF at 0.2C (c).

However, the surface of lithium anode is uniform with PNTF addition (Fig. 7c), demonstrating that the addition of PNTF evidently inhibit the dissolution and migration of lithium polysulfides in the electrolyte. Thus the corrosion reaction between lithium anode and PS is suppressed effectively.

4. Conclusion

PPy nanotubes film is self-assembled with a simple method from PPy nano-tubes. As the functional interlayer of Li–S battery, PNTF can not only reduce the polarization of the cell, but also suppress the shuttle effect during charge/discharge process because of the strong adsorption effect between PPy and lithium polysulfides. Moreover, PNTF has higher specific area and larger amount of pores compared to those of PFIL, thus it shows bigger advantages when it is used as the functional interlayer. Thus the strategy adapted here can be helpful to the commercialization of Li–S battery. New functional interlayer for Li–S battery, such as the other conductive polymers, Li^+ conductor ceramic and so on, are all worth studying in the future.

Acknowledgments

This work was financially supported by NSFC Project No. 51373195, No. 51372262, No. 51201177 and No. 51272267; research projects from the Science and Technology Commission of Shanghai Municipality No. 08DZ2210900.

We thank Prof. B. V. R. Chowdari (Department of Physics, National University of Singapore) for helpful discussions.

References

[1] Stefan A. Freunberger, Peter G. Bruce, Laurence J. Hardwick, Jean-Marie Tarascon, Nat. Mater. 11 (1) (2012) 19.
[2] Y.X. Yin, S. Xin, Y.G. Guo, L.J. Wan, Angew. Chem. Int. Ed. 52 (50) (2013) 13186.
[3] D.-W. Wang, Q. Zeng, G. Zhou, L. Yin, F. Li, H.-M. Cheng, I.R. Gentle, G.Q.M. Lu, J. Mater. Chem. A 1 (2013) 9382.
[4] S.S. Zhang, Electrochem. Commun. 31 (2013) 10–12.
[5] Y. Yang, G. Zheng, Y. Cui, Chem. Soc. Rev. 42 (2013) 3018.
[6] A. Manthiram, Y. Fu, S.-H. Chung, C. Zu, Y.-S. Su, Chem. Rev. (2014), 140715153614001.
[7] G. Xu, B. Ding, J. Pan, P. Nie, L. Shen, X. Zhang, J. Mater. Chem. A 2 (2014) 12662.
[8] S. Moon, Y.H. Jung, W.K. Jung, D.S. Jung, J.W. Choi, D.K. Kim, Adv. Mater. 25 (45) (2013) 6547–6553.
[9] Y. Mao, H. Duan, B. Xu, L. Zhang, Y. Hu, C. Zhao, Z. Wang, L. Chen, Y. Yang, Energy Environ. Sci. 5 (2012) 7950.
[10] W. Zhou, Y. Yu, H. Chen, F.J. DiSalvo, H.D. Abruña, J. Am. Chem. Soc. 135 (2013) 16736–16743.
[11] X. Liang, Z.Y. Wen, Y. Liu, M.F. Wu, J. Jin, H. Zhang, X.W. Wu, J. Power Sources 196 (2011) 9839.
[12] G. Ma, Z. Wen, J. Jin, M. Wu, G. zhang, X. Wu, J. Zhang, Solid State Ionics 262 (2014) 174–178.
[13] L. Suo, Y.-S. Hu, H. Li, M. Armand, L. Chen, Nat. Commun. 4 (2013) 1481.
[14] J.-W. Park, K. Yamauchi, E. Takashima, N. Tachikawa, K. Ueno, K. Dokko, M. Watanabe, J. Phys. Chem. C 117 (2013) 4431–4440.
[15] Y.-S. Su, A. Manthiram, Nat. Commun. 3 (2012) 1166.
[16] Y.-S. Su, A. Manthiram, Chem. Commun. 48 (2012) 8817.
[17] X. Wang, Z. Wang, L. Chen, J. Power Sources 242 (2013) 65–69.
[18] C. Zu, Y.-S. Su, Y. Fu, A. Manthiram, Phys. Chem. Chem. Phys. 15 (2013) 2291.
[19] H. Chen, W. Dong, J. Ge, C. Wang, X. Wu, W. Lu, L. Chen, Sci. Rep. 3 (2013) 01910–01915.
[20] L. Xiao, Y. Cao, J. Xiao, B. Schwenzer, M.H. Engelhard, L.V. Saraf, Z. Nie, G.J. Exarhos, J. Liu, Adv. Mater. 24 (2012) 1176–1181.
[21] G. Ma, Z. Wen, J. Jin, Y. Lu, X. Wu, M. Wu, C. Chen, J. Mater. Chem. A 2 (2014) 10350.
[22] G. Ma, Z. Wen, J. Jin, Y. Lu, X. Wu, C. Liu, C. Chen, RSC Adv. 4 (2014) 21612.
[23] C. Wang, W. Wan, J.-T. Chen, H.-H. Zhou, X.-X. Zhang, L.-X. Yuan, Y.-H. Huang, J. Mater. Chem. A 1 (2013) 1716.
[24] F. Wu, J. Chen, R. Chen, S. Wu, L. Li, S. Chen, T. Zhao, J. Phys. Chem. C 115 (2011) 6057–6063.
[25] S.S. Zhang, J. Power Sources 231 (2013) 153–162.
[26] G. Ma, Z. Wen, J. Jin, M. Wu, X. Wu, J. Zhang, J. Power Sources 267 (2014) 542–546.
[27] X. Liang, Y. Liu, Z. Wen, L. Huang, X. Wang, H. Zhang, J. Power Sources 196 (2011) 6951–6955.
[28] X.M. Yang, Z.X. Zhu, T.Y. Dai, Y. Lu, Macromol. Rapid Comm. 26 (2005) 1736–1740.
[29] R. Xu, I. Belharouak, J.C.M. Li, X. Zhang, I. Bloom, J. Bareño, Adv. Energy Mater. 3 (2013) 833–838.
[30] J. Zheng, M. Gu, C. Wang, P. Zuo, P.K. Koech, J.G. Zhang, J. Liu, J. Xiao, J. Electrochem. Soc. 160 (2013) A1992–A1996.
[31] Y. Diao, K. Xie, S. Xiong, X. Hong, J. Electrochem. Soc. 159 (2012) A1816–A1821.
[32] N.A. Cañas, K. Hirose, B. Pascucci, N. Wagner, K.A. Friedrich, R. Hiesgen, Electrochim Acta 97 (2013) 42–51.
[33] Z. Deng, Z. Zhang, Y. Lai, J. Liu, J. Li, Y. Liu, J. Electrochem. Soc. 160 (2013) A553–A558.
[34] J. Zheng, D. Lv, M. Gu, C. Wang, J.G. Zhang, J. Liu, J. Xiao, J. Electrochem. Soc. 160 (2013) A2288–A2292.